549158

5B.4 DOPPLER AND REFLECTIVITY MEASUREMENTS AT TWO CLOSELY-SPACED FREQUENCIES

R. Meneghini[1], S. Bidwell[1], L. Liao[2], G. Heymsfield[1], R. Rincon[3], and A. Tokay[4]

[1]NASA/Goddard Space Flight Center, Greenbelt, MD
[2]Caelum Research Corp., Rockville, MD
[3]George Washington University, Washington, D.C.
[4]JCET, UMBC, Baltimore, MD

1. INTRODUCTION

Spaceborne and airborne radars are limited with respect to the mass and size of the instrument and the power available to operate it. As a consequence, dual-wavelength radars that require separate antennas and power amplifiers are expensive and often impractical. However, if the frequency difference can be reduced so that a single antenna and the same radio-frequency subsystem can be used for both frequencies, dual-wavelength Doppler measurements can be made with a radar of about the same size and mass as its single-frequency counterpart.

In the first part of the paper we present calculations of the reflectivity factor differences as functions of the center frequency from 10 to 35 GHz and for frequency differences between −10% and 10% of the center frequency. The results indicate that differential-frequency operation at Ka-band frequencies (26.5 – 40 GHz) provides relatively strong differential signals if the frequencies can be separated by at least 5%. Unlike lower frequency operation, the differential signals at Ka-band (both reflectivity and Doppler) are directly related to the median mass diameter. An important feature of the differential mean Doppler is that it depends only on the drop-size dependent part of the radial velocity. In principle, the mean and mean differential Doppler data from a nadir-looking platform can be used to infer vertical air motion and characteristics of the particle size distribution (Meneghini et al., 2001).

To test the instrument concept, the ER-2 Doppler radar (Heymsfield et al., 1996) was modified for differential frequency operation. Measurements by the modified radar, operating at frequencies of 9.1 GHz and 10 GHz, were made using an 8^0 zenith-pointing offset parabolic antenna. Simultaneous data were taken with an optical rain gauge and an impact disdrometer. Measured and DSD-estimated values of the differential dBZ mean Doppler are presented in section 3.

2. DIFFERENTIAL FREQUENCY CALCULATIONS

For the results shown here, the hydrometeors are taken to be spherical and the scattering cross sections are calculated from Mie theory. We define the equivalent reflectivity factor difference, $\delta Z_e(f, \delta f)$, or more simply, the differential reflectivity, by

$$\delta Z_e(f, \delta f) = \mathrm{sgn}(\delta f)\,[dBZ_e(f) - dBZ_e(f+\delta f)] \qquad (1)$$

where sgn(x) = 1 for x>0 and −1 for x<0 so that δZ_e is always taken as the difference between dBZ_e at the lower frequency to that at the higher frequency. The equivalent reflectivity factor at frequency f is given by $dBZ_e(f) = 10 \log_{10} Z_e(f)$ where

$$Z_e(f) = \lambda^4/[\pi^5|K_w|^2] \int \sigma_b(\lambda, D)\, N(D)\, dD \qquad (2)$$

where $\sigma_b(\lambda, D)$ is the backscattering cross section (mm^2) of a spherical particle of diameter D at wavelength λ and where N(D) is the drop size distribution ($mm^{-1}\, m^{-3}$). For the calculations presented, N(D) is assumed to be an exponential. Because δZ_e is proportional to the log of a ratio of Z_e measurements, it is independent of number concentration but dependent on the median mass diameter, D_0. The differential mean Doppler, $\delta v(f, \delta f)$, can be defined in a similar way:

$$\delta v(f, \delta f) = \mathrm{sgn}(\delta f)\,[\langle v(f)\rangle - \langle v(f+\delta f)\rangle] \qquad (3)$$

where $\langle v(f)\rangle$ is the mean Doppler velocity at the radar frequency f. Shown in Fig. 1 are contour plots of δZ_e

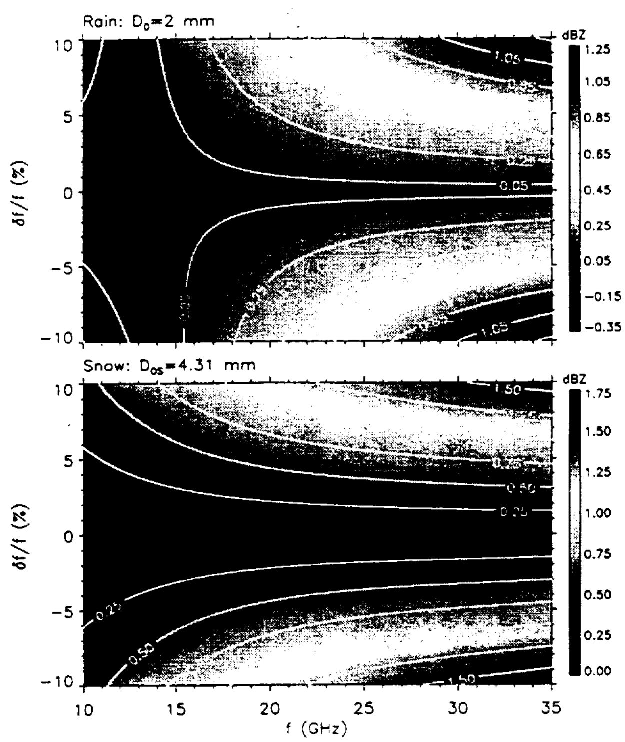

Fig. 1: Contour plots of δZ_e in the f-δf space for rain with D_0=2 mm (top) and snow with D_{0s}=4.31 mm (bottom).

* *Corresponding author address:* Robert Meneghini, NASA/GSFC, Code 975, Greenbelt, MD 20771; e-mail: bob@priam.gsfc.nasa.gov.

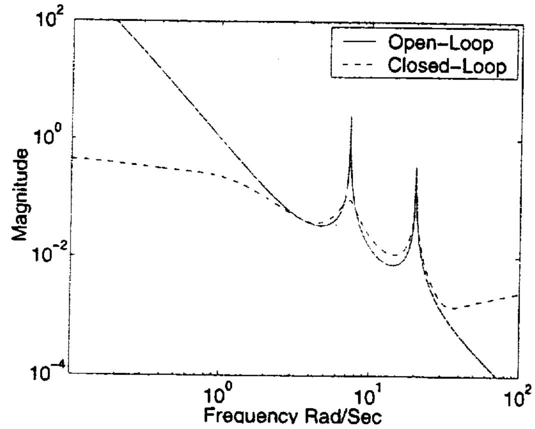

(a) Fully coupled performance/robustness path

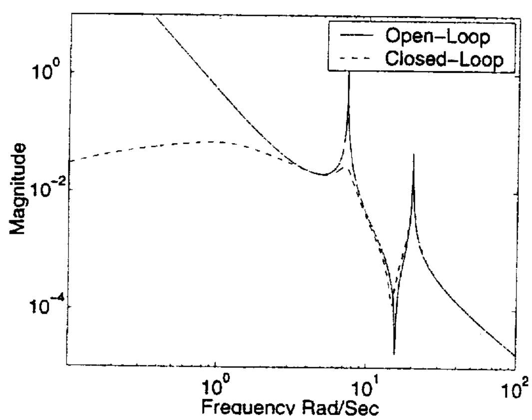

(b) Performance path only

Fig. 3 Maximum singular value plot for open and nominal closed loop system.

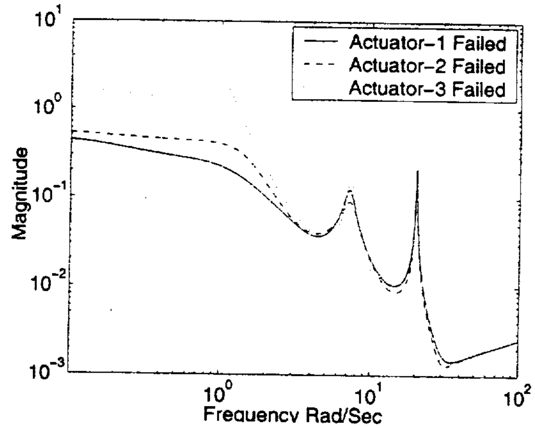

(a) Fully coupled performance/robustness path

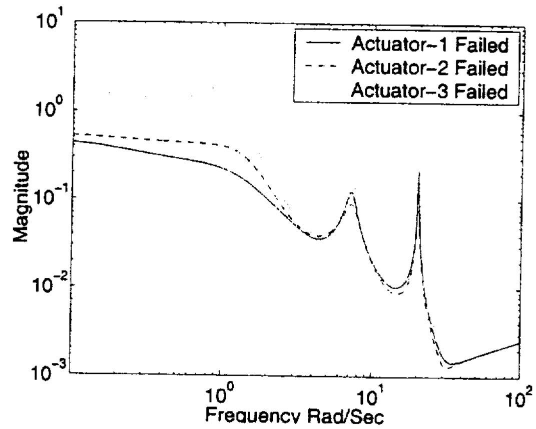

(b) Performance path only

Fig. 5 Maximum singular value plot for closed-loop system under different actuator failures

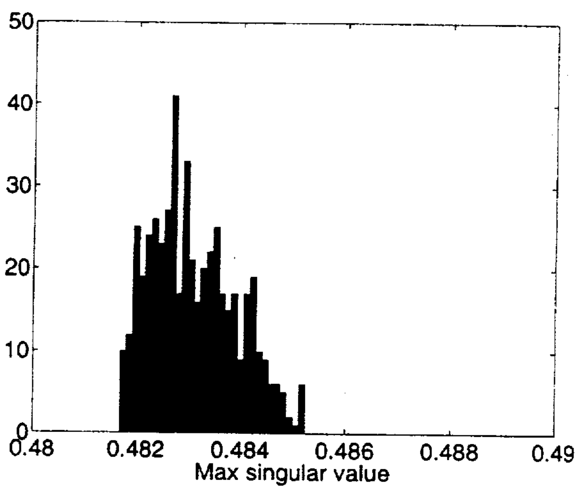

Fig. 4 Variation of H_∞ norm with 5% errors in natural frequency, 500 cases

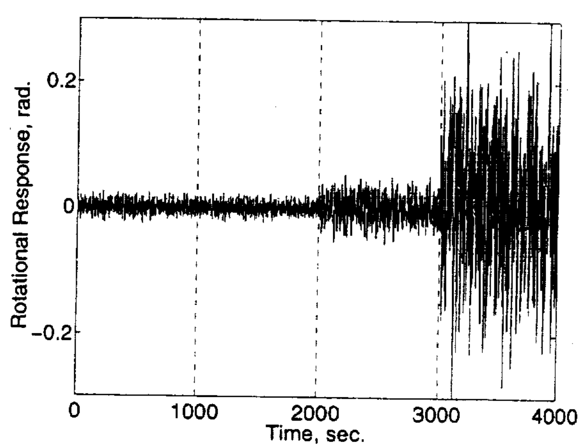

Fig. 6 Time response of pointing under disturbance for four conditions: Operational, Act-1 Failure, Act-2 Failure, and Act-3 Failure

note that there are 3 mechanisms at work. In rain, at X-band frequencies, δZ_e is negative, i.e., dBZ_e increases locally with f. Generally speaking, larger D_0 values are associated with larger values of $|\delta Z_e|$ although it must be noted that $|\delta Z_e|$ attains a maximum at $D_0 \approx 1.8$ mm and begins to decrease thereafter. As the signals propagate into the rain δZ_e becomes progressively less negative because the attenuation at the higher frequency is larger than that at the lower. Because δZ_e is positive in dry snow, a change in the sign of δZ_e occurs as the signals transit the melting layer.

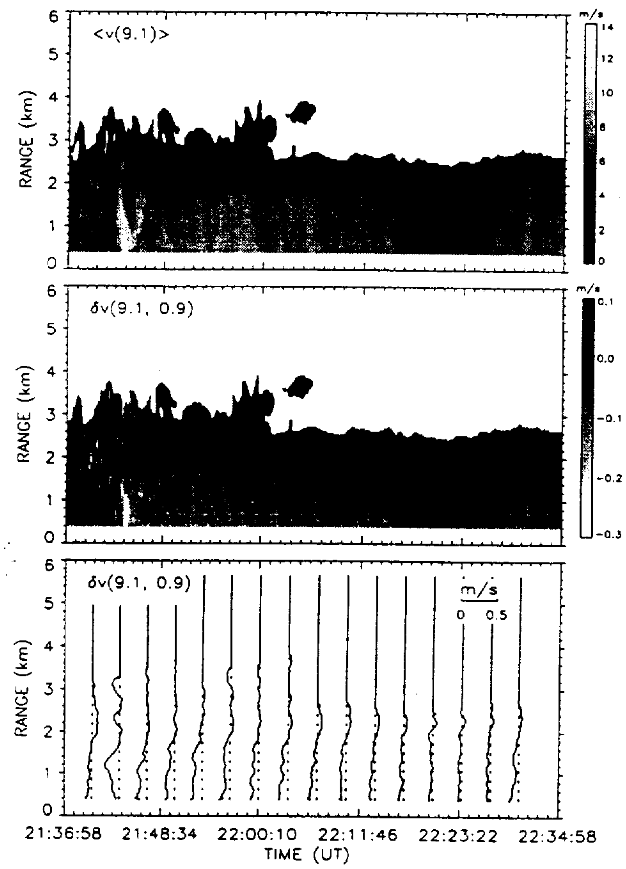

Fig. 4. Height-time plots of <v(9.1 GHz)> (top), δv(9.1, 0.9) (center) and height-profiles of δv (bottom).

Somewhat similar characteristics can be seen in the differential mean Doppler results pictured in the center and lower panels of Fig. 4. In contrast to δZ_e, δv is insensitive to differential attenuation. Moreover, δv is approximately zero in the snow region.

To validate the measurement concept, it is important to show the relation between the differential signals and the drop size distributions. To do this, we have used the disdrometer data and Mie theory to calculate the expected values of dBZ_e, δZ_e, <v> and δv. An example of comparisons between the disdrometer-derived dBZ_e and δZ_e and the corresponding EDOP measurements is shown in Fig. 5. A 60-s shift of the EDOP data was introduced to account for the fact that the EDOP data were taken at a 400m height. Although comparisons

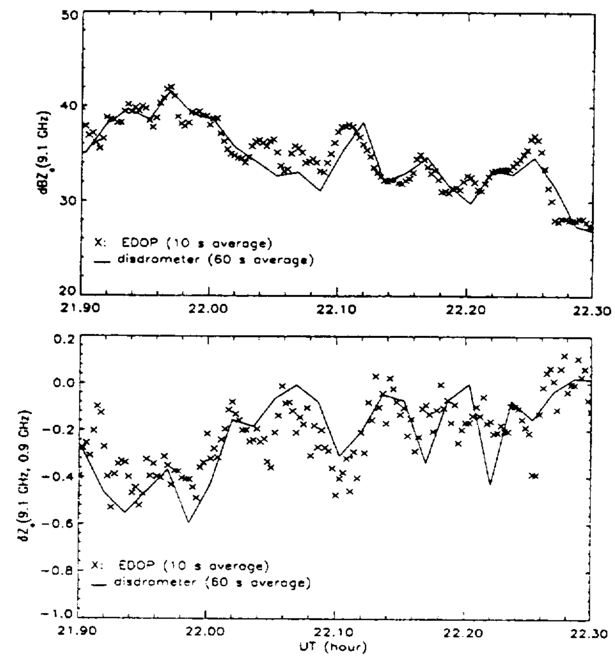

Fig. 5: Comparisons of EDOP measurements (X) and disdrometer-derived (solid lines) values of dBZ(9.1 GHz) (top) and δZ_e(9.1 GHz, 0.9 GHz) over a 24 min period.

between the EDOP data and DSD-derived estimates of δZ_e are noisy, the correlation is relatively good. This is encouraging in the sense that the (9.1 GHz, 10 GHz) combination is far from optimum, suggesting that sets of frequencies at Ka-band, separated by 5% to 10%, should yield stable estimates of δZ_e and δv.

4. SUMMARY

Computations of the differential-frequency radar reflectivity factor and mean Doppler suggest that useful information on the drop size distribution and vertical air motion are feasible at Ka-band frequencies where the signal levels are relatively strong and directly related to the median drop diameter. As such, the measurement concept has applications to airborne and spaceborne sensing of rain and cloud. Experimental tests of the concept were conducted using the X-band EDOP radar where it was shown that measurements of δZ_e correlate fairly well with estimates derived from measured drop size distributions.

5. REFERENCES

Bidwell, S.W. et al., 2000: Application of a differential reflectivity technique to the EDOP radar in ground-based operation. *Proc. IGARSS2000*, Honolulu, HI.

Heymsfield, G.M. et al., 1996: The EDOP radar system on the high-altitude NASA ER-2 aircraft. *J. Atmos and Oceanic Technol.*, **13**, 795-809.

Meneghini, R., L. Liao, S. Bidwell, and G.M Heymsfield, 2001: On the feasibility of a Doppler weather radar for estimates of DSD using two closely-spaced frequencies, *TGARS* (submitted).

for rain (top) and snow (bottom) cases. For example, the values of δZ_e for the frequency pair (25 GHz, 26.25 GHz) can be found at the (x, y) coordinates (25 GHz, +5%) yielding δZ_e= 0.45 dB in the case of rain and δZ_e= 0.6 dB for snow. For a fixed center frequency we can examine the behavior of δZ_e in the δf–D_0 space by contour plots of the type shown in Fig. 2. Comparisons of the 14 and 35 GHz results reveal two advantages of

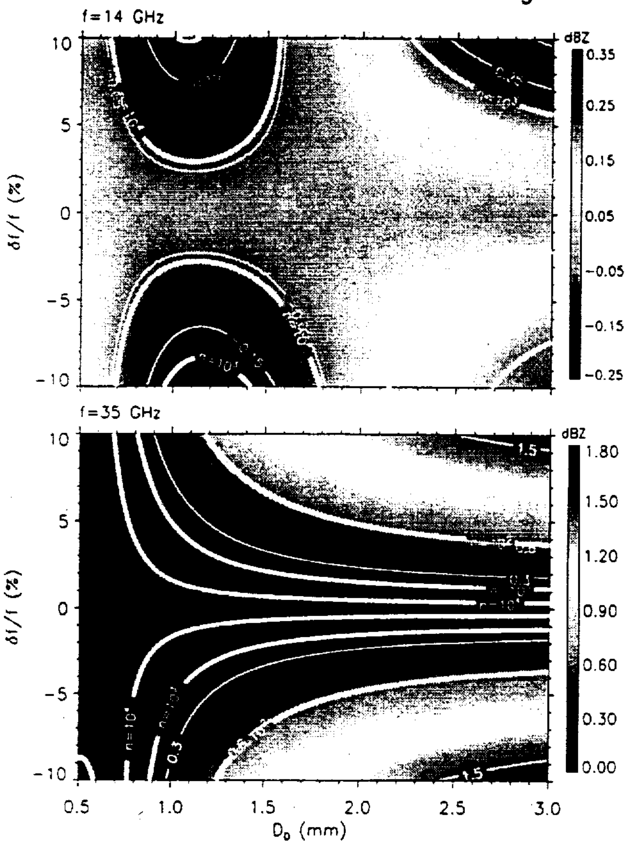

Fig. 2: Contour plots of δZ_e in δf –D_0 space for fixed center frequencies of 14 GHz (top) and 35 GHz(bottom).

operating at the higher frequency: larger signal strength and a 1-to-1 relationship between δZ_e and D_0. At 14 GHz, in contrast, more than one value of D_0 is consistent with the δZ_e measurement over certain ranges. Contours of n, the number of independent samples required for the mean differential signal level to be greater than the standard deviation of the measurement, are also shown on the figures.

3. EDOP DIFFERENTIAL MEASUREMENTS

Differential frequency measurements were made using the ER-2 Doppler radar (EDOP) in a ground-based, zenith-looking configuration. To modify the EDOP for differential measurements, the local oscillator (LO) at 9.6 GHz was disconnected and replaced with two synthesized HP-83640 sweep generators. These oscillators were used both to generate the transmit pulse and to mix the received signals down to the intermediate frequency (IF). The LO frequencies were chosen to produce transmit frequencies of 9.1 and 10 GHz, a separation that was found to be the practical limit based on the performance characteristics of the EDOP traveling wave tube amplifier (TWTA). It should be noted that the generation, transmission, and reception of the two frequencies were done simultaneously (Bidwell et al., 2000).

On March 27, 2000, an impact disdrometer and optical rain gauge were placed next to the zenith-directed antenna. Approximately 3 hours of data were collected. Because the modified radar was uncalibrated, the radar return powers were converted into radar reflectivities, by an additive constant, using the drop size distribution data near the beginning of the measurement period. Height versus time plots of dBZ_e(9.1 GHz) and δZ_e(f=9.1 GHz, δf = 0.9 GHz) are shown in the top and center panels of Fig. 3. Displayed in the bottom panel are selected vertical profiles of δZ_e. Corresponding plots of <v(9.1 GHz)> and δv(9.1, 0.9) are shown in Fig. 4. The data show that the rain was primarily stratiform with a well-defined bright-band at a height of approximately 2.2 km. To understand the δZ_e

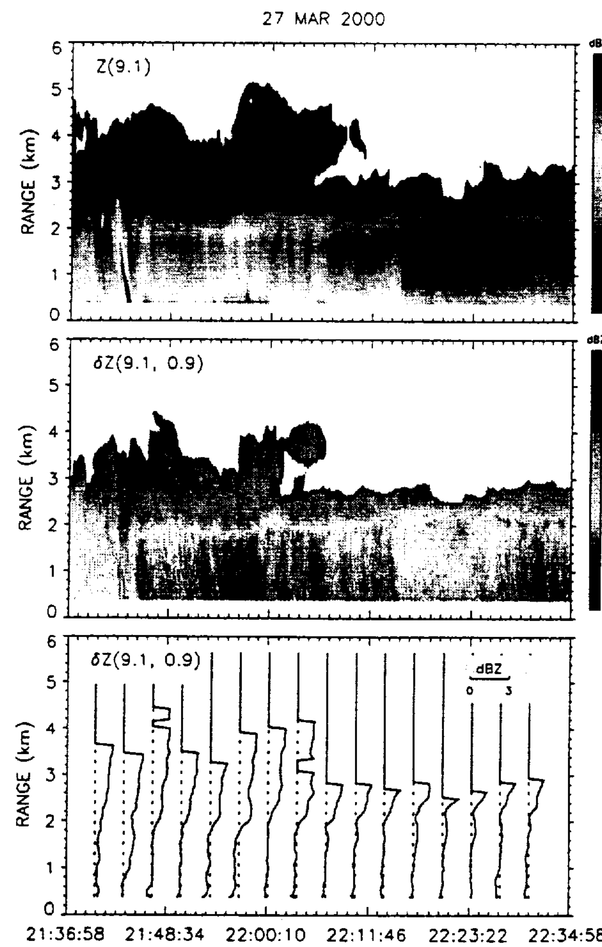

Fig. 3. Height-time plots of dBZ_e(9.1 GHz) (top), δZ_e(9.1 GHz, 0.9 GHz) (center) and height-profiles of δZ_e (bottom).